



# TOI-1994b: A Low-mass Eccentric Brown Dwarf Transiting A Subgiant Star

Emma Page<sup>1</sup> , Joshua Pepper<sup>1</sup> , Duncan Wright<sup>2</sup> , Joseph E. Rodriguez<sup>3</sup> , Robert A. Wittenmyer<sup>2</sup> , Stephen R. Kane<sup>4</sup> , Brett Addison<sup>2,5</sup> , Timothy Bedding<sup>6</sup> , Brendan P. Bowler<sup>7</sup> , Thomas Barclay<sup>8,9</sup> , Karen A. Collins<sup>10</sup> , Phil Evans<sup>11</sup> , Jonathan Horner<sup>12</sup> , Eric L. N. Jensen<sup>13</sup> , Marshall C. Johnson<sup>14</sup> , John Kielkopf<sup>15</sup> , Ismael Mireles<sup>16</sup> , Peter Plavchan<sup>17</sup> , Samuel N. Quinn<sup>10</sup> , S. Seager<sup>18,19,20</sup> , Avi Shporer<sup>18</sup> , Keivan G. Stassun<sup>21</sup> , Stephanie Striegel<sup>22</sup> , Joshua N. Winn<sup>23</sup> , George Zhou<sup>2</sup> , and Carl Ziegler<sup>24</sup>

<sup>1</sup> Department of Physics, Lehigh University, 16 Memorial Drive East, Bethlehem, PA 18015, USA; [ejp520@lehigh.edu](mailto:ejp520@lehigh.edu)

<sup>2</sup> University of Southern Queensland, Centre for Astrophysics, USQ Toowoomba, West Street, QLD 4350 Australia

<sup>3</sup> Center for Data Intensive and Time Domain Astronomy, Department of Physics and Astronomy, Michigan State University, East Lansing, MI 48824, USA

<sup>4</sup> Department of Earth and Planetary Sciences, University of California, Riverside, CA 92521, USA

<sup>5</sup> Swinburne University of Technology, Centre for Astrophysics and Supercomputing, John Street, Hawthorn, VIC 3122, Australia

<sup>6</sup> School of Physics, Sydney Institute for Astronomy (SIFA), The University of Sydney, NSW 2006, Australia

<sup>7</sup> Department of Astronomy, The University of Texas at Austin, TX 78712, USA

<sup>8</sup> NASA Goddard Space Flight Center, 8800 Greenbelt Road, Greenbelt, MD 20771, USA

<sup>9</sup> University of Maryland, Baltimore County, 1000 Hilltop Circle, Baltimore, MD 21250, USA

<sup>10</sup> Center for Astrophysics | Harvard & Smithsonian, 60 Garden Street, Cambridge, MA 02138, USA

<sup>11</sup> El Sauce Observatory, Coquimbo Province, Chile

<sup>12</sup> University of Southern Queensland, Centre for Astrophysics, West Street, Toowoomba, QLD 4350 Australia

<sup>13</sup> Department of Physics & Astronomy, Swarthmore College, Swarthmore PA 19081, USA

<sup>14</sup> Department of Astronomy, The Ohio State University, 4055 McPherson Laboratory, 140 West 18<sup>th</sup> Avenue, Columbus, OH 43210 USA

<sup>15</sup> Department of Physics and Astronomy, University of Louisville, Louisville, KY 40292, USA

<sup>16</sup> Department of Physics and Astronomy, University of New Mexico, 210 Yale Boulevard NE, Albuquerque, NM 87106, USA

<sup>17</sup> George Mason University, 4400 University Drive MS 3F3, Fairfax, VA 22030, USA

<sup>18</sup> Department of Physics and Kavli Institute for Astrophysics and Space Research, Massachusetts Institute of Technology, Cambridge, MA 02139, USA

<sup>19</sup> Department of Earth, Atmospheric and Planetary Sciences, Massachusetts Institute of Technology, Cambridge, MA 02139, USA

<sup>20</sup> Department of Aeronautics and Astronautics, MIT, 77 Massachusetts Avenue, Cambridge, MA 02139, USA

<sup>21</sup> Department of Physics and Astronomy, Vanderbilt University, Nashville, TN 37235, USA

<sup>22</sup> SETI Institute, Mountain View CA 94043/NASA Ames Research Center, Moffett Field, CA 94035, USA

<sup>23</sup> Department of Astrophysical Sciences, Princeton University, Princeton, NJ 08544, USA

<sup>24</sup> Department of Physics, Engineering and Astronomy, Stephen F. Austin State University, 1936 North Street, Nacogdoches, TX 75962, USA

Received 2023 May 11; revised 2023 December 3; accepted 2023 December 4; published 2024 February 14

## Abstract

We present the discovery of TOI-1994b, a low-mass brown dwarf transiting a hot subgiant star on a moderately eccentric orbit. TOI-1994 has an effective temperature of  $7700^{+720}_{-410}$  K,  $V$  magnitude of 10.51 mag and  $\log(g)$  of  $3.982^{+0.067}_{-0.065}$ . The brown dwarf has a mass of  $22.1^{+2.6}_{-2.5} M_J$ , a period of 4.034 days, an eccentricity of  $0.341^{+0.054}_{-0.059}$ , and a radius of  $1.220^{+0.082}_{-0.071} R_J$ . TOI-1994b is more eccentric than other transiting brown dwarfs with similar masses and periods. The population of low-mass brown dwarfs may have properties similar to planetary systems if they were formed in the same way, but the short orbital period and high eccentricity of TOI-1994b may contrast this theory. An evolved host provides a valuable opportunity to understand the influence stellar evolution has on the substellar companion's fundamental properties. With precise age, mass, and radius, the global analysis and characterization of TOI-1994b augments the small number of transiting brown dwarfs and allows the testing of substellar evolution models.

*Unified Astronomy Thesaurus concepts:* [Brown dwarfs \(185\)](#); [Photometry \(1234\)](#); [Radial velocity \(1332\)](#); [Substellar companion stars \(1648\)](#)

*Supporting material:* machine-readable table

## 1. Introduction

Brown dwarfs are substellar objects that burn deuterium for up to 1 Gyr and have masses between those of planets and stars (Spiegel et al. 2011). A compact object's ability to burn deuterium is primarily defined by the mass of the object, but the most common definition is debated in the astronomical community. The International Astronomical Union (IAU) uses the limiting mass for thermonuclear fusion of deuterium as the

lower limit for brown dwarfs, which is around  $13 M_J$  for objects of solar metallicity (Boss 2007).

There are arguments that the definition of a brown dwarf should instead be based on formation mechanisms rather than mass. They suggest that massive planets can burn deuterium similar to brown dwarfs, and that the two domains overlap when using the IAU definition. This new definition, based on formation mechanisms of brown dwarfs, considers whether the substellar object possibly formed more like a star or like a planet. This suggests that the brown dwarf regime is simply the tail end of the planetary and stellar formation mechanisms. Solidifying this definition proves to be difficult since formation theory is incomplete, the boundary between formation mechanisms is unclear, and we have no definitive way of

knowing how a particular object formed (Burrows et al. 2001; Grieves et al. 2021).

It is possible that different formation mechanisms lead to different populations of brown dwarf companions. Ma & Ge (2014) discovered that the brown dwarf population can be split at around  $42.5 M_J$  based on eccentricity. Lower-mass brown dwarfs display an eccentricity distribution consistent with massive planets (Rodriguez et al. 2023), while higher-mass brown dwarfs have an eccentricity distribution similar to binary stars (Halbwachs et al. 2003). This could suggest that brown dwarfs with mass  $<42.5 M_J$  form similar to planets in protoplanetary disks and  $>42.5 M_J$  form similarly to stellar binaries (although see Schlaufman (2018) for an alternate proposal to this boundary). More recent studies found a similar brown dwarf eccentricity distributions using larger populations (Grieves et al. 2017, 2021; Kiefer et al. 2021).

Compared to giant planets and stars, brown dwarfs are less often detected as short-period companions around main sequence stars (Grether & Lineweaver 2006; Sahlmann et al. 2011). Although this result is slowly changing in recent years due to space-based photometry, brown dwarfs still have a lower occurrence rate according to more recent studies (e.g., Grieves et al. 2017; Kiefer et al. 2021). The lack of brown dwarf companions with periods less than 100 days is commonly referred to as the “brown dwarf desert.” This desert may be caused by the different formation mechanisms for low-mass and high-mass brown dwarfs. The transition point between planet formation and binary star formation is not fully understood. Well characterized brown dwarf companions are required to provide insight into the brown dwarf desert and formation mechanisms. Specifically, transiting brown dwarf companions with precisely calculated radii are quite valuable. With a tight age, and precise brown dwarf mass, radius, and eccentricity, we can directly test substellar evolution models (e.g., Baraffe et al. 2003; Phillips et al. 2020).

Space-based photometric missions make discovering transiting brown dwarfs more accessible. The Transiting Exoplanet Survey Satellite (TESS; Ricker et al. 2015) is a space-based photometric survey with a primary mission of discovering transiting exoplanets. TESS was launched in 2018 and has currently confirmed 330 planets with over 6400 planet candidates identified as of 2023 April 24<sup>25</sup>, as well as monitoring known exoplanetary systems (Kane et al. 2021). In addition to planets, TESS is able to detect transiting brown dwarf companions. Out of the 39 confirmed transiting brown dwarf companions currently known, TESS has discovered almost half (Grieves et al. 2021; Cañas et al. 2022; Carmichael et al. 2022; Lin et al. 2023; Psaridi et al. 2022; Sebastian et al. 2022; Vowell et al. 2023). The use of TESS to detect transiting brown dwarf companions enables the determination of precise radii, and may therefore illuminate the brown dwarf desert and associated formation mechanisms.

We report the discovery of TOI-1994b, a low-mass brown dwarf with moderate eccentricity transiting an evolved star. TOI-1994b is one of only six known brown dwarf companions transiting an evolved star (Carmichael et al. 2021; Lin et al. 2023; Psaridi et al. 2022). The moderate eccentricity of TOI-1994b may present a discrepancy with previous attempts to define brown dwarfs using eccentricity distributions to determine formation mechanisms.

In Section 2, we present the TESS discovery and spectroscopic follow-up observations for TOI-1994b. Section 3 describes the EXOFASTv2 global fit and presents final parameters for the TOI-1994 system. Section 4 discusses the ways that TOI-1994b is unique and how it compares to other brown dwarf companions.

## 2. Discovery and Follow-up Observations

### 2.1. TESS Discovery

TESS<sup>26</sup> (Ricker et al. 2015) is a near all-sky photometric survey searching for exoplanets transiting mainly nearby bright main sequence stars. TESS splits most of the sky into sectors and observes each for a minimum time baseline of 27 days. During the first two years of the mission, TESS observed about 160,000 selected stars at a 2 minute cadence, and obtained 30 minute cadence full-frame images (FFIs) for the entire sector region. In July of 2022, TESS completed its primary mission and began its first Extended Mission which switched to a 10 minute cadence for FFIs. Starting in September of 2022, TESS began its second Extended Mission and increased the cadence for the FFIs to 200 s.

TESS observed TESS Input Catalog (TIC) 445903569 in sectors 9 and 10 in February and March of 2019, and sector 36 in March of 2021<sup>27</sup>. TESS obtained 30 minute FFIs in sectors 9 and 10 and 10 minutes FFIs in sector 36. In addition, TIC 445903569 was observed during sector 36 in 2 minute cadence. Initial transits were detected by the Quick-Look Pipeline (QLP; Huang et al. 2020a, 2020b) using data taken from the 30 minutes FFIs from sectors 9 and 10. In October of 2021, the TESS Follow-up Program (TFOP; Collins et al. 2018) team at MIT identified TIC 445903569 as a host-star candidate using the QLP light curves, and designated it TOI-1994 using the procedure described in Guerrero et al. (2021). The later 2 minute cadence TESS observations from sector 36 were processed using the Science Processing Operations Center (SPOC; Jenkins et al. 2016) pipeline from the NASA Ames Research Center, which produced PDC-SAP light curves we used (Smith et al. 2012; Stumpe et al. 2012, 2014). SPOC conducted a transit search of Sector 36 on 2021 April 14 with an adaptive, noise-compensating matched filter (Jenkins 2002; Jenkins et al. 2010, 2020), producing a threshold crossing event for which an initial limb-darkened transit model was fitted (Li et al. 2019), and a suite of diagnostic tests were conducted to help make or break the planetary nature of the signal (Twicken et al. 2018). The signal was repeatedly recovered as additional observations were made in sectors 62 and 63, and the transit signature passed all the diagnostic tests presented in the Data Validation reports produced by SPOC for this target (Jenkins et al. 2016). We used the `lightkurve` python package (Lightkurve Collaboration et al. 2018) to collect the light curves from the Mikulski Archive for Space Telescopes (MAST) and flattened the data using `Keplerspline`.<sup>28</sup>

Figures 1 and 2 show the light curves of TIC 445903569 from the SPOC and QLP pipelines. There is a dilution in the TESS light curves of 14%. The transits have a depth of 3.23

<sup>26</sup> All the TESS data used in this paper can be found in MAST (10.17909/t9-nmc8-f686 and 10.17909/t9-r086-e880).

<sup>27</sup> TIC 445903569 was also observed in sectors 62 and 63 after the time of writing. Visual inspection shows consistency with the results reported here.

<sup>28</sup> <https://github.com/avanderburg/keplerspline>

<sup>25</sup> <https://exoplanetarchive.ipac.caltech.edu/>

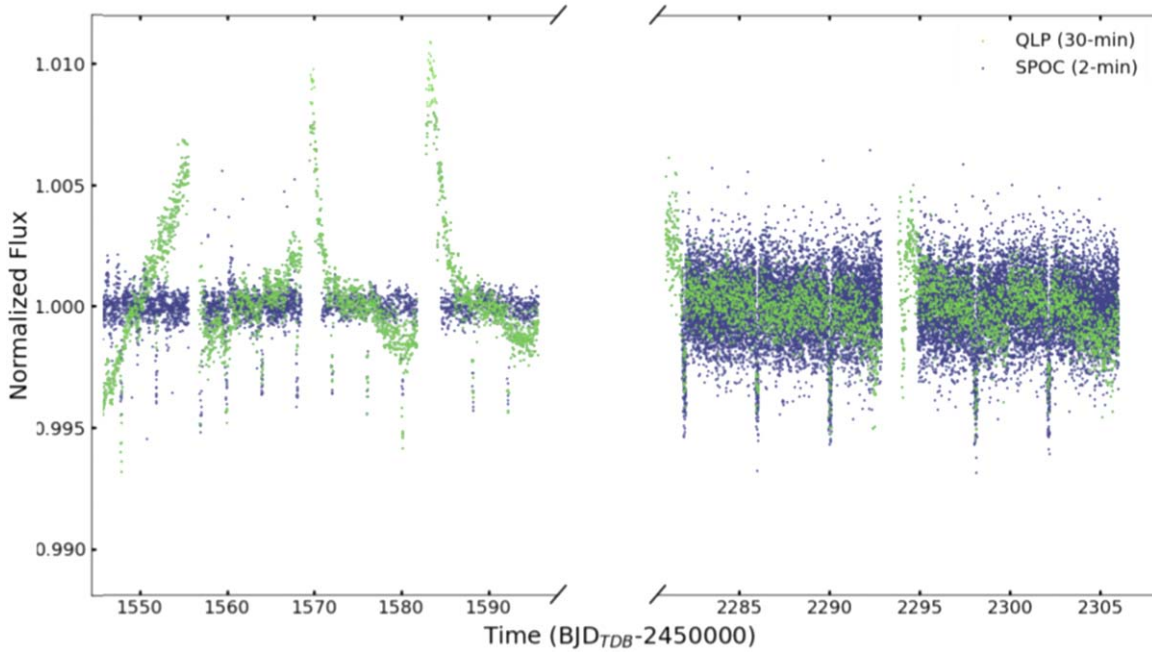


**Figure 1.** Discovery light curves from TESS for TOI-1994b using 2 minute cadence data from the SPOC pipeline from Sector 36 (blue dots) and 30 minute cadence data from the QLP pipeline from Sectors 9 and 10 (green diamonds).

parts per thousand, a period of 4.0337142 days, and duration of 3.82 hr.

## 2.2. Follow-up Photometry

We acquired ground-based time-series photometry as part of TFOP (Collins et al. 2018). We used the TESS Transit Finder, a customized version of the Tapir software package (Jensen 2013) to schedule our observations.

We observed three transit events with the Las Cumbres Observatory Global Telescope Network (LCOGT; Brown et al. 2013) 1 m telescopes and Sinistro cameras. We observed an egress on 2020 November 23 in the  $z$  band from the Siding Spring Observatory node, a full transit on 2021 February 8 in  $z$  from Cerro Tololo Interamerican Observatory (CTIO), and a full transit minus egress on 2021 February 15 in  $B$ , again from CTIO. The data were reduced using the LCOGT facility BANZAI pipeline (McCully et al. 2018), and the light curves extracted using AstroImageJ (Collins et al. 2017).

We observed a full transit in Johnson-Cousins  $R_c$ -band on 2021 February 7 using the Evans 0.36 m telescope at El Sauce Observatory in Coquimbo Province, Chile. The telescope was equipped with a ST1603-3 CCD camera with  $1536 \times 1024$  pixels binned  $2 \times 2$  in-camera resulting in an image scale of  $1''.47 \text{ pixel}^{-1}$ . The photometric data was obtained from a set of  $116 \times 25$  s exposures, followed by a set of  $870 \times 30$  s exposures (exposure time adjusted to improve the S/N before the start of ingress) after standard calibration, using a circular  $7''.4$  aperture in AstroImageJ (Collins et al. 2017).

We jointly modeled all three ground-based light curves (taken in the  $B$ ,  $R_c$ , and PANSTARRS  $z$ -short passbands) and allowed the dilution to vary independently for two of the bands relative to the third, mimicking the case where the occulting body or a third source contributes significantly to the observed light curve. Figure 3 displays these three ground-based light curves and the joint model. We find all dilution factors to be statistically consistent, i.e., showing no indication

of differential dilution in the different photometric apertures. We then fit the light curves with no dilution and found  $R_p/R_* = 0.053^{+0.002}_{-0.001}$ , which is within  $1\sigma$  of the  $R_p/R_*$  value found from the EXOFASTv2 global fit, confirming consistency with the TESS aperture crowding correction factor. We also find an orbital period of  $P = 4.03$  days, which is within  $2\sigma$  of the period we find from the joint model of the TESS plus radial velocity data in the global fit.

These ground-based photometry showed that the transit occurred on-target on the expected host star, and was achromatic, thus helping to vet the candidate for further follow-up observations.

## 2.3. Spectroscopic Observations

To measure the mass of the transiting object, we obtained high-resolution spectroscopy of TOI-1994 from ground-based telescopes to extract radial velocities (RVs).

TOI-1994b was spectroscopically observed by the MINERVA-Australis telescope array in Toowoomba, Australia at the University of Southern Queensland’s Mount Kent Observatory. The telescopes T3, T4 and T5 were used for spectroscopic observations of TOI-1994. Each MINERVA-Australis telescope uses fiber optic cables to feed light into a spectrograph reaching resolution  $R = 80000$  for wavelengths from 480 to 630 nm (Addison et al. 2019).

A total of 47 spectra were taken by MINERVA-Australis between 2021 June 5 and 2021 July 12 with an exposure time of 3600 s.

We also collected a 23 measurements with the CHIRON spectrograph (Tokovinin et al. 2013) on the 1.5 m SMARTS telescope at CTIO in Chile. The observations were obtained between 2021 November 6 and 2022 May 1, resulting in full phase coverage for the orbit of TOI-1994b. We employed the fiber-fed image slicer to yield a resolving power of  $R \sim 80,000$  between 4100 and 8700 Å. The typical exposure time was 800 s and resulted in a mean S/N per resolution element of 65. We

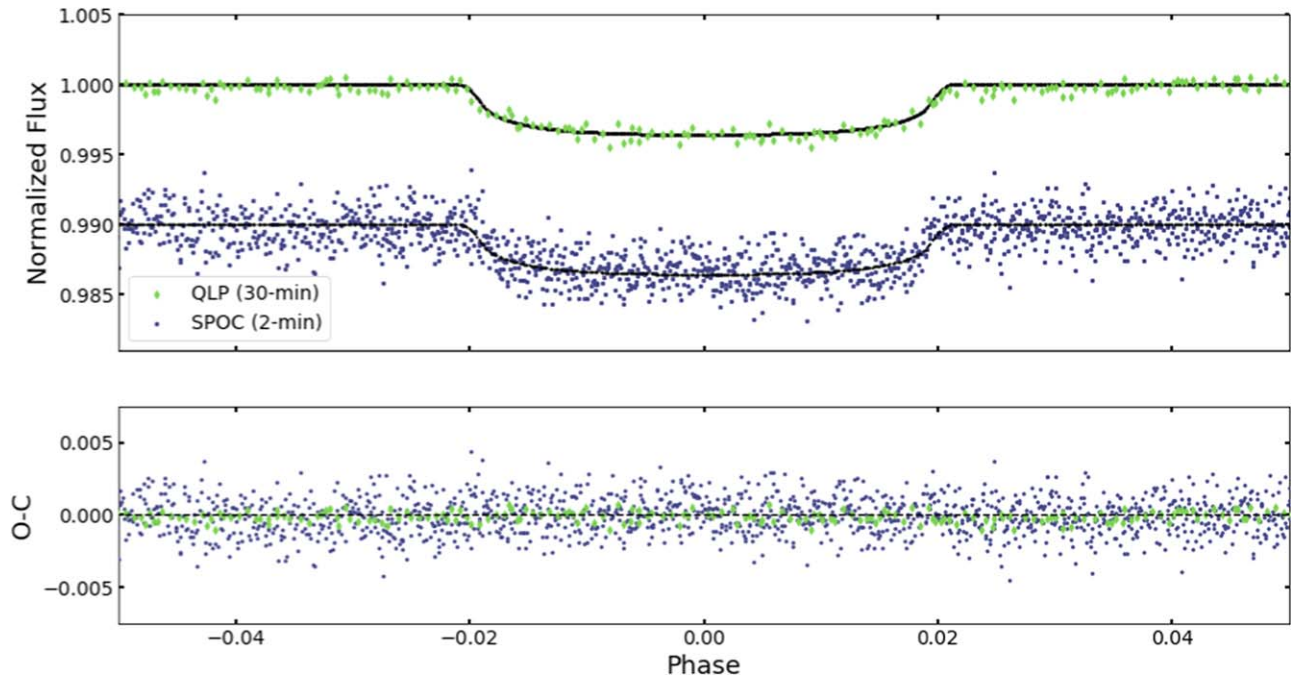


**Figure 2.** Discovery light curves from TESS for TOI-1994b using 2 minutes cadence data from the SPOC pipeline from Sector 36 (blue dots) and 30 minutes cadence data from the QLP pipeline from Sectors 9 and 10 (green diamonds). The black line represents a model fit from the EXOFASTv2 described in Section 3. The curves are phase folded to a period of 4.0337142 days. The residuals for the best fit model are shown in the bottom panel.

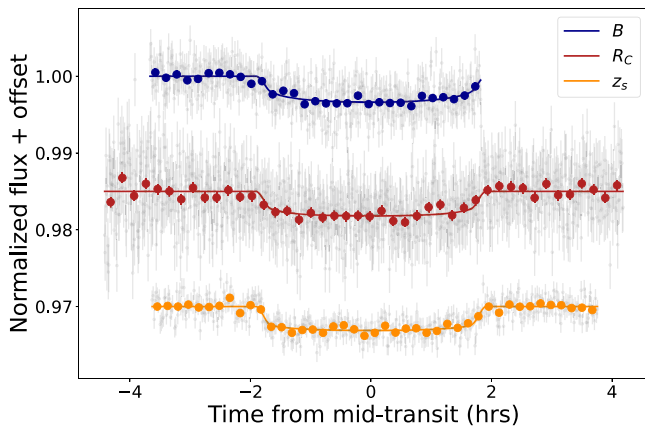


**Figure 3.** Ground-based light curves taken in  $B$ ,  $R_c$  and PANSTARRS  $z_s$ -short passbands plotted with corresponding models. The depth of the transit is consistent across these passbands.

used the optimal extraction provided by the CHIRON team, described in Paredes et al. (2021), and extracted radial velocities by fitting line profiles derived by least-squares deconvolution of the observed spectra against synthetic templates (Donati et al. 1997; Zhou et al. 2020).

We note that TOI-1994 is fast-rotating, with  $v \sin i > 45 \text{ km s}^{-1}$ . This makes it difficult to extract reliable stellar parameters from the spectra (such as  $T_{\text{eff}}$ ,  $\log g$ , and  $[\text{Fe}/\text{H}]$ ), and affects the RV precision we are able to achieve. In the global fit below, we adopt stellar parameters from the TIC for starting points of the analysis.

The first ten radial velocities from the MINERVA-Australis telescope array and CHIRON are listed in Table 1. The full list of RV observations are available online as a machine-readable table. The RVs with the best fit model are shown in Figure 4 phase folded using the period and epoch from the EXOFASTv2 global analysis described in Section 3.

**Table 1**  
Radial Velocity Observations of TOI-1994

BJD <sub>TDB</sub> - 2450000.0	RV (m s <sup>-1</sup> )	$\sigma_{\text{RV}}$ (m s <sup>-1</sup> )	Facility
9370.97041 ...	-2600	750	MINERVA T3
9370.97041 ...	-2000	710	MINERVA T5
9370.97041 ...	-3740	910	MINERVA T4
9377.92662 ...	-150	770	MINERVA T3
9377.92662 ...	1000	450	MINERVA T5
9524.84483 ...	-1160	700	CHIRON
9533.84916 ...	376	520	CHIRON
9533.86065 ...	220	466	CHIRON
9535.86140 ...	715	510	CHIRON
9537.85895 ...	369	755	CHIRON

(This table is available in its entirety in machine-readable form.)

#### 2.4. SOAR Speckle High-resolution Imaging

The presence of unresolved luminous sources can complicate the characterization of a transiting system by diluting the true transit depth, or even creating a false positive signal (Ciardi et al. 2015). To search for any such companions, we used high-resolution speckle imaging.

TOI-1994 was observed by the 4.1 m Southern Astrophysical Research (SOAR) telescope using the  $I$  filter on October 31st, 2020. A description of the instrument is found in Tokovinin (2018) and observation details are described in Ziegler et al. (2021). Figure 5 displays the  $5\sigma$  detection sensitivity and inset autocorrelation function (ACF) taken on 2020 October 31 from SOAR.

The speckle observations are sensitive to companion objects down to a  $\Delta \text{ mag}$  of 6.5 at  $1''$ . These observations show that there are no close stellar companions within  $3''$  of TOI-1994. We therefore rule out the possibility of a false positive caused by a nearby stellar companion.

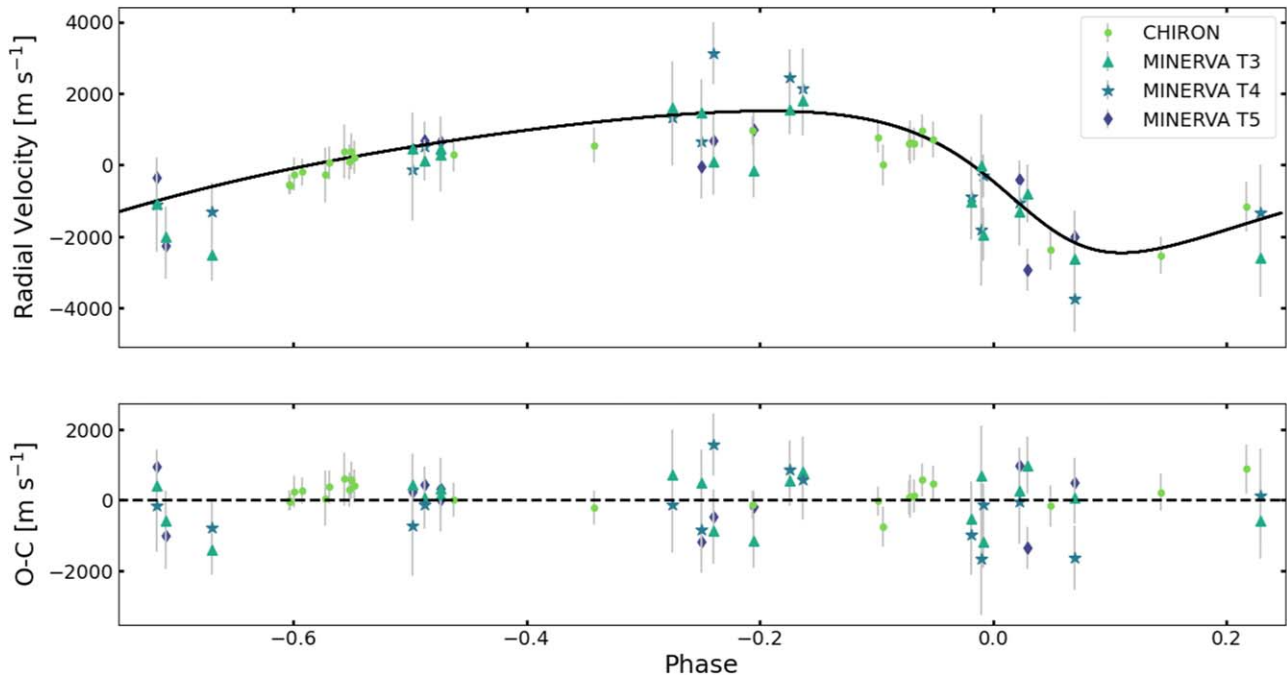


**Figure 4.** Radial velocities for TOI-1994 from CHIRON and three MINERVA-Australis telescopes. The black line represents the global fit model from the EXOFASTv2 described in Section 3. The curve is phase folded to a period of 4.0337142 days. The residuals for the best-fit model are shown below the radial velocity curve.

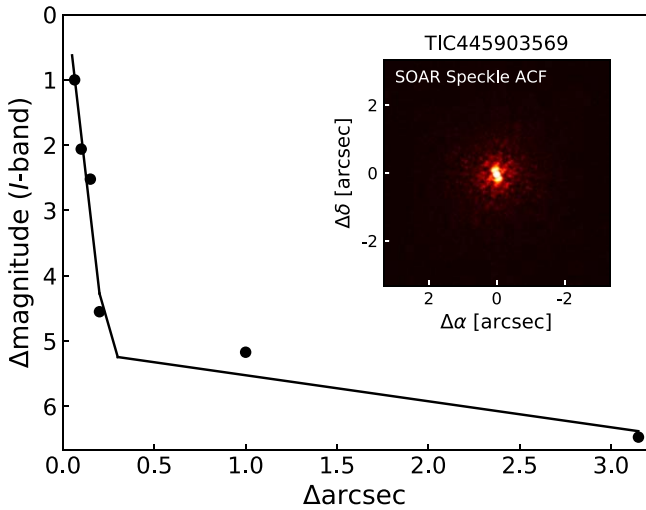


**Figure 5.** Speckle imaging from SOAR of TOI-1994. The points represent  $5\sigma$  detection sensitivity and the inset displays ACF from SOAR. No stellar companions are found within  $3''$  down to the detection limits.

### 3. EXOFASTv2 Global Fits

We simultaneously modeled the transit photometry and RVs using EXOFASTv2, an exoplanet-fitting software package written in IDL (Eastman et al. 2013; Eastman 2017; Eastman et al. 2019). This tool allows us to fit multiple data sets simultaneously using a Markov chain Monte Carlo analysis.

EXOFASTv2 uses starting points for stellar properties, the spectral energy distribution, and MESA Isochrones and Stellar Tracks (MIST) in order to model the host star (Choi et al. 2016; Dotter 2016). The spectral energy distribution we used as a part of the global model in EXOFASTv2 is given in Table 2.

We began the global modeling process by running an initial EXOFASTv2 fit using the TESS photometry and the RVs from the CHIRON spectrograph on the SMARTS 1.5 m telescope

discussed in Sections 2.1 and 2.3. We prepared the data for EXOFASTv2 using astropy (Astropy Collaboration et al. 2013, 2018, 2022). This initial fit used starting points as uniform priors for stellar mass, radius and effective temperature from the TIC (Stassun et al. 2018, 2019), and the period and epoch from TESS photometry. We placed a wide Gaussian prior of  $[\text{Fe}/\text{H}] = 0.0 \pm 1$  dex on metallicity, a Gaussian prior of  $\varpi = 1.94140 \pm 0.04211$  mas from Gaia DR2 on parallax, and an upper limit of 2.64275 on  $V$ -band extinction from Schlegel et al. (1998) and Schlafly & Finkbeiner (2011).

We ran another fit using EXOFASTv2 that incorporated everything from the initial fit, with the addition of RVs from the MINERVA-Australis telescope array, described in Section 2.3. Each MINERVA-Australis telescope was fit as a separate spectrograph since the systematics are not consistent between them. The purpose of this second run was to fit for a slope over time in the RV data from both facilities. If a slope is detected, it could be a sign of a stellar companion with a much longer orbital period than TOI-1994b. This fit was consistent with a slope of zero over the 350 day baseline. Thus, the final fit presented here does not include a slope over time for the RV data.

The final fit, presented here, used TESS photometry, and RVs from the MINERVA-Australis telescope array and the CHIRON spectrograph on the SMARTS 1.5 m telescope. The description of this data is found in Section 2. This fit used starting point for stellar properties, period, and epoch from the initial EXOFASTv2 fit. The same MIST evolution models and SED starting points described for the initial fit were used in this final fit. We used a smaller Gaussian prior on metallicity of  $[\text{Fe}/\text{H}] = 0.0 \pm 0.5$  dex based on the results from the initial fit. We placed the same Gaussian prior on parallax from Gaia DR2, and the same upper limit on  $V$ -band extinction described previously. The starting points and priors used in the final EXOFASTv2 fit are listed in Table 3.

**Table 2**  
Properties From Literature

Identifiers:			
	TOI ...	TOI-1994	
	TIC ...	TIC 445903569	
	TYCHO-2 ...	TYC 8193-1368-1	
	2MASS ...	J09484191-5145236	
	HD ...	HD 298656	
Parameter	Description	Value	Reference
$\alpha$ ...	R.A. (J2000, epoch 2015.5) ...	09:48:41.9	Gaia Collaboration et al. (2023)
$\delta$ ...	decl. (J2000, epoch 2015.5) ...	-51:45:23.63	Gaia Collaboration et al. (2023)
T ...	TESS mag ...	10.2396 $\pm$ 0.0061	Stassun et al. (2018, 2019)
G ...	Gaia G mag ...	10.4280 $\pm$ 0.0200	Gaia Collaboration et al. (2023)
$B_P$ ...	Gaia $B_P$ mag ...	10.5787 $\pm$ 0.0200	Gaia Collaboration et al. (2023)
$R_P$ ...	Gaia $R_P$ mag ...	10.1965 $\pm$ 0.0200	Gaia Collaboration et al. (2023)
$J$ ...	2MASS $J$ mag ...	9.915 $\pm$ 0.024	Cutri et al. (2003)
$H$ ...	2MASS $H$ mag ...	9.843 $\pm$ 0.023	Cutri et al. (2003)
$K_S$ ...	2MASS $K_S$ mag ...	9.775 $\pm$ 0.021	Cutri et al. (2003)
WISE1...	WISE1 mag ...	9.767 $\pm$ 0.030	Cutri et al. (2012)
WISE2...	WISE mag ...	9.823 $\pm$ 0.030	Cutri et al. (2012)
WISE3...	WISE3 mag...	10.041 $\pm$ 0.049	Cutri et al. (2012)
$\mu_\alpha$ ...	Gaia DR3 proper motion in R.A. (mas yr <sup>-1</sup> )...	-13.547 $\pm$ 0.0577	Gaia Collaboration et al. (2023)
$\mu_\delta$ ...	Gaia DR3 proper motion in decl. (mas yr <sup>-1</sup> )	-1.741 $\pm$ 0.064	Gaia Collaboration et al. (2023)
$\varpi$ ...	Gaia DR3 Parallax (mas) ...	1.94140 $\pm$ 0.04211	Gaia Collaboration et al. (2023)

Figure 2 displays the best-fit model for the TESS light curves in black, and Figure 4 shows the best-fit radial velocity model in black. Table 3 lists the derived stellar parameters and brown dwarf parameters from the final EXOFASTv2 global fit.

From the EXOFASTv2 global fit analysis, we find that TOI-1994 is a hot, fast-rotating subgiant with a radius of  $2.30^{+0.13}_{-0.12} R_\odot$ , mass of  $1.86^{+0.18}_{-0.17} M_\odot$ , effective temperature of  $7700^{+720}_{-410}$  K, and surface gravity of  $3.982^{+0.067}_{-0.065} \text{ cm s}^{-2}$ .

The effective temperature and luminosity of TOI-1994 places it near the center of the instability strip for  $\delta$  Scuti pulsations. Figure 6 displays TOI-1994 on a Hertzsprung–Russell (HR) diagram with other transiting brown dwarf hosts (see Section 4 for further information on this population). The instability strip is plotted as given by Dupret et al. (2005), and shows the position of TOI-1994. Based on studies with Kepler (e.g., Bowman & Kurtz 2018; Murphy et al. 2019), this implies a probability of around 50%–70% that TOI-1994 pulsates as a  $\delta$  Scuti variable. We carried out Fourier analysis of the TESS light curve (using the residuals from the transit fit) on both the 2 minute and 30 minute data, but found no evidence for pulsations down to an amplitude limit of about 50 parts per million.

#### 4. Discussion

We present the discovery of TOI-1994b, a low-mass brown dwarf transiting an evolved host star with a moderately eccentric orbit. We now compare TOI-1994b to 38 other transiting brown dwarf systems shown in Figures 7, 8, and 9. We gathered properties for these other transiting brown dwarf systems from Cañas et al. (2022), Carmichael et al. (2022), Lin et al. (2023), Psaridi et al. (2022), Sebastian et al. (2022), Vowell et al. (2023), and Grieves et al. (2021; see references therein). We define a brown dwarf as a substellar object between  $13M_J$  and  $80M_J$  for this discussion. We note that five of the transiting brown dwarfs in this sample are in triple

systems (Irwin et al. 2010; Johnson et al. 2011; Nowak et al. 2017; Irwin et al. 2018; Jackman et al. 2019).

Figure 7 shows TOI-1994b on the mass–radius diagram with 38 other transiting brown dwarfs with masses between 13 and  $80 M_J$ . We also show isochrones for brown dwarfs that have cooled due to the lack of hydrogen fusion with ages 0.1, 0.5, 1, 5, and 10 Gyr (Baraffe et al. 2003). Age affects the radius of a brown dwarf depending on its mass, with older objects having smaller radii. We note that there is further work being done in order to refine radii of transiting brown dwarfs, such as Carmichael (2023).

We determine a tight age constraint of  $0.94^{+0.33}_{-0.31}$  Gyr using MIST models in the EXOFASTv2 fit, since TOI-1994 is a subgiant star. We expect that the brown dwarf companion formed at the same time as its stellar host and also has an age of 0.94 Gyr. Using the tight age constraint, along with precise mass, radius, and eccentricity, we can directly test substellar evolution models. Substellar evolutionary models predict that brown dwarfs are formed with inflated radii and then contract. This contraction rate starts off rapidly and then decreases over  $\sim 10$  Gyr (e.g., Baraffe et al. 2003; Phillips et al. 2020). In Figure 7, TOI-1994b falls along a younger isochrone of 0.1 Gyr. This indicates that the radius of TOI-1994b is larger than the models predict for a 0.94 Gyr brown dwarf. It is not clear whether TOI-1994b experienced reinflation, or has remained inflated despite the rapid contraction after formation predicted by substellar models. The larger radius of TOI-1994b may be caused by an increase in luminosity of the host star causing reinflation as it evolves off the main sequence. This is a method of reinflation proposed for hot-giant planets as in Thorngren et al. (2021) and Lopez & Fortney (2016). However, planet mass may affect reinflation, with less massive objects experiencing more dramatic inflation for objects up to  $13 M_J$  (Thorngren & Fortney 2018; Thorngren et al. 2021). If this trend is expected to continue for brown dwarf masses, this may suggest that the inflated brown dwarfs shown in Figure 7 are not experiencing the same type of reinflation as giant planets.

**Table 3**  
Median Values and 68% Confidence Intervals for the EXOFASTv2 Global Model

Symbol	Parameter	Value
Priors:		
$P_{\dots}$	Period (days)...	4.0337
$T_{C0\dots}$	Epoch (BJD <sub>TDB</sub> )...	2459290.01406
$\varpi_{\dots}$	Parallax <sup>a</sup> (mas) ...	$1.94140 \pm 0.04211$
[Fe/H]...	Metallicity <sup>a</sup> (dex)...	$0.0 \pm 0.5$
$A_V_{\dots}$	V-band extinction <sup>b</sup> (mag)...	2.64275
Stellar parameters:		
$M_{*}\dots$	Mass ( $M_{\odot}$ )...	$1.86^{+0.18}_{-0.17}$
$R_{*}\dots$	Radius ( $R_{\odot}$ )...	$2.30^{+0.13}_{-0.12}$
$L_{*}\dots$	Luminosity ( $L_{\odot}$ )...	$16.7^{+6.3}_{-2.7}$
$F_{Bol}\dots$	Bolometric flux $\times 10^{-9}$ ( $10^9$ erg s <sup>-1</sup> cm <sup>-2</sup> )...	$1.99^{+0.74}_{-0.31}$
$\rho_{*}\dots$	Density (g cm <sup>-3</sup> )...	$0.215^{+0.047}_{-0.038}$
$\log g_{\dots}$	Surface gravity (cm s <sup>-2</sup> )...	$3.982^{+0.067}_{-0.065}$
$T_{eff}\dots$	Effective temperature (K)...	$7700^{+720}_{-410}$
[Fe/H]...	Metallicity (dex)...	$-0.01^{+0.30}_{-0.42}$
[Fe/H] <sub>0</sub> ...	Initial metallicity <sup>c</sup> ...	$0.07^{+0.28}_{-0.41}$
Age...	Age (Gyr)...	$0.94^{+0.33}_{-0.31}$
EEP...	Equal evolutionary Phase <sup>d</sup> ...	$361^{+26}_{-15}$
$A_V_{\dots}$	V-band extinction (mag)...	$0.22^{+0.29}_{-0.16}$
$\sigma_{SED}\dots$	SED photometry error scaling ...	$2.67^{+1.2}_{-0.67}$
$\varpi_{\dots}$	Parallax (mas)...	$1.931 \pm 0.042$
$d_{\dots}$	Distance (pc)...	$517^{+12}_{-11}$
Brown dwarf parameters:		
$P_{\dots}$	Period (days)...	$4.0337142 \pm 0.0000051$
$R_p_{\dots}$	Radius ( $R_J$ )...	$1.220^{+0.082}_{-0.071}$
$M_p_{\dots}$	Mass ( $M_J$ )...	$22.1^{+2.6}_{-2.5}$
$T_C_{\dots}$	Time of conjunction (BJD <sub>TDB</sub> )...	$2459290.01375^{+0.00079}_{-0.00084}$
$T_0_{\dots}$	Optimal conjunction time <sup>e</sup> (BJD <sub>TDB</sub> )...	$2458854.37263^{+0.00056}_{-0.00064}$
$a_{\dots}$	Semimajor axis (AU)...	$0.0613 \pm 0.0019$
$i_{\dots}$	Inclination (Degrees)...	$85.5^{+2.9}_{-2.5}$
$e_{\dots}$	Eccentricity ...	$0.341^{+0.054}_{-0.059}$
$\tau_{circ}\dots$	Tidal circularization timescale (Gyr)...	$4.2^{+3.9}_{-2.1}$
$\omega_{*}\dots$	Argument of periastron (Degrees)...	$131.6^{+7.9}_{-6.7}$
$T_{eq}\dots$	Equilibrium temperature (K)...	$2290^{+170}_{-110}$
$K_{\dots}$	RV semiamplitude (m s <sup>-1</sup> )...	$1970 \pm 170$
$R_p/R_{*}\dots$	Radius of planet in stellar radii ...	$0.05449^{+0.0012}_{-0.00084}$
$a/R_{*}\dots$	Semimajor axis in stellar radii ...	$5.72^{+0.39}_{-0.36}$
$\delta_{\dots}$	$(R_p/R_*)^2$ ...	$0.002969^{+0.00013}_{-0.000091}$
$\delta_{TESS} \dots$	Transit depth in TESS (fraction)...	$0.00328^{+0.00027}_{-0.00019}$
$\tau_{\dots}$	Ingress/egress transit duration (days)...	$0.00970^{+0.0020}_{-0.00095}$
$T_{14}\dots$	Total transit duration (days)...	$0.1685^{+0.0021}_{-0.0019}$
$b_{\dots}$	Transit Impact parameter ...	$0.32^{+0.17}_{-0.20}$
$T_{S,14}\dots$	Total eclipse duration (days)...	$0.249^{+0.047}_{-0.049}$
$\rho_p_{\dots}$	Density (g cm <sup>-3</sup> )...	$15.0^{+3.9}_{-3.2}$
$\log g_p_{\dots}$	Surface gravity (cm s <sup>-2</sup> ) ...	$4.564^{+0.078}_{-0.080}$
$T_S_{\dots}$	Time of eclipse (BJD <sub>TDB</sub> )...	$2459291.445^{+0.097}_{-0.10}$
$e \cos \omega_{*}\dots$	...	$-0.222^{+0.036}_{-0.038}$
$e \sin \omega_{*}\dots$	...	$0.255^{+0.056}_{-0.064}$
$d/R_{*}\dots$	Separation at midtransit ...	$4.02^{+0.61}_{-0.51}$

**Notes.**<sup>a</sup> Indicates a Gaussian prior.<sup>b</sup> Indicates an upper limit.<sup>c</sup> The Initial Metallicity is the metallicity of the star when it was formed.<sup>d</sup> The Equal Evolutionary Point corresponds to static points in a stars evolutionary history when using the MIST isochrones and can be a proxy for age. See 2 in Dotter (2016) for a more detailed description of EEP.<sup>e</sup> Optimal time of conjunction minimizes the covariance between  $T_C$  and Period. This is the transit midpoint.

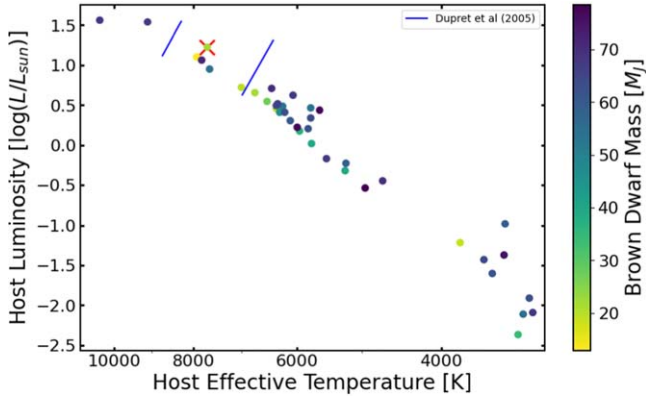


**Figure 6.** HR diagram for 39 transiting brown dwarf companions. TOI-1994b is marked with a red “x.” The solid blue lines represent the instability strip as given by Dupret et al. (2005). Points are colored by the mass of the brown dwarf companions.

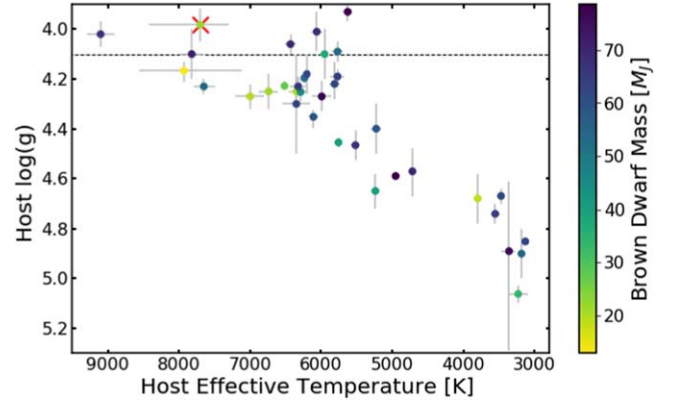


**Figure 9.** Surface gravity and effective temperature of 39 stars hosting transiting brown dwarf companions. The colors indicate the mass of the brown dwarf companions. TOI-1994b is marked with a red “x.” The horizontal dashed line indicates  $\log(g) = 4.1$  as the transition between main sequence and evolved giant stars as in Stassun et al. (2018).

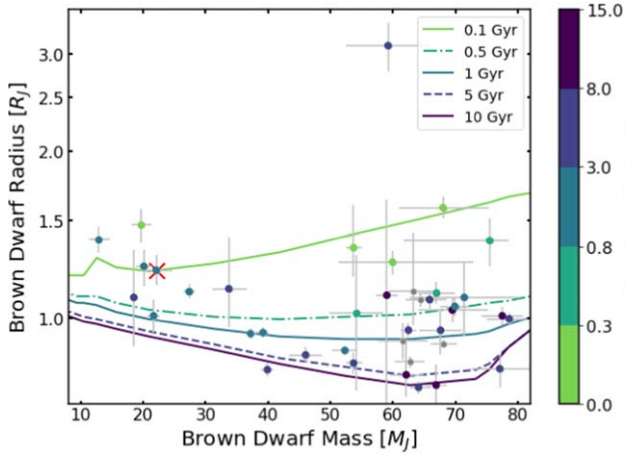


**Figure 7.** Mass–radius diagram for 39 transiting brown dwarf companions. TOI-1994b is marked with a red “x.” The colored lines represent isochrones for brown dwarfs at ages 0.1, 0.5, 1, 5, and 10 Gyr (Baraffe et al. 2003). Points are colored by the age of the system from publications. Gray represents systems published with a large age range.

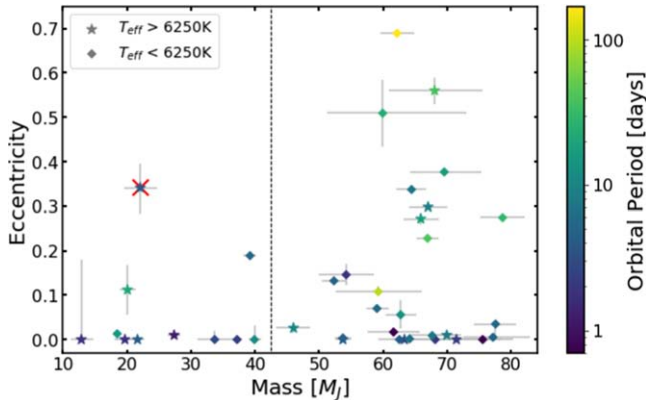


**Figure 8.** Eccentricity vs. brown dwarf mass for 39 transiting brown dwarf companions. The color represents the orbital period of the system. Squares represent hosts with temperatures below the Kraft break ( $T_{\text{eff}} \approx 6250$ ) and stars represent hosts with temperatures above the Kraft break. A vertical line shows the population split at  $42.5 M_J$  proposed by Ma & Ge (2014). TOI-1994b is marked with a red “x.”

Additionally, as pointed out in Bodenheimer et al. (2001), tidal heating of short-period planets in eccentric orbits can cause inflated radii. As such, it is possible that the inflated radius of

TOI-1994b can be explained by its orbital dynamics. It is possible that the same mechanisms that cause inflated radii in giant planets are also driving inflated radii in brown dwarfs. However, more brown dwarfs with precise parameters such as age, mass, and radius are necessary to test substellar evolution models and confirm whether planet inflation mechanisms can extend to include brown dwarfs.

In addition to radius and mass, period and eccentricity also give insight to the dynamical nature of the transiting system. The orbital eccentricity for close-in planets and stars with orbital periods less than  $\sim 10$  days may become circularized from interactions with their host stars over longer timescales (Goldreich & Soter 1966; Hut 1981; Adams & Laughlin 2006).

With an age of 0.94 Gyr and period of 4.03 days, we explore whether the system should be circularized. Since TOI-1994 is a subgiant star, we expect that the slightly larger radius and stronger tides will cause a shorter circularization timescale. In order to estimate the circularization timescale,  $\tau_{\text{circ}}$ , for TOI-1994b, we used Equation (3) from Adams & Laughlin (2006):

$$\tau_{\text{circ}} \approx 1.6[\text{Gyr}] \left( \frac{Q_p}{10^6} \right) \left( \frac{M_p}{M_J} \right) \times \left( \frac{M_*}{M_\odot} \right)^{-3/2} \left( \frac{R_p}{R_J} \right)^{-5} \left( \frac{a}{0.05[\text{AU}]} \right)^{13/2}. \quad (1)$$

We used the EXOFASTv2 values from Table 3, and an estimate of  $\frac{Q_p}{10^6} \approx 1$  where  $Q_p$  is the tidal quality factor. The tidal quality factor is between  $10^5 < Q_p < 10^6$  for gaseous planets (Goldreich & Soter 1966). Using these parameters, we found that the circularization timescale for TOI-1994b is 4.2 Gyr, with large uncertainties of +3.9 and  $-2.1$  Gyr. However, even with the large uncertainty, the  $1\sigma$  lower bound is still greater than the age of TOI-1994b of  $0.94^{+0.33}_{-0.31}$  Gyr found using the global analysis. Thus, using  $Q_p = 10^6$ , we would not expect the system to be circularized. This is confirmed by the eccentricity of  $0.314^{+0.054}_{-0.059}$ .

Beatty et al. (2018) estimated a  $Q_p > 10^{4.15}$  for a  $36.5 M_J$  transiting brown dwarf. If we adopt  $Q_p = 10^{4.15}$  for TOI-1994b, we find that the circularization timescale is 0.06 Gyr. However, large uncertainties in the true value of  $Q_p$  for both planets and brown dwarfs make it difficult to use such constraints for a particular system.



TOI-1994b is moderately eccentric compared to other brown dwarfs with similar mass and orbital period. Figure 8 displays the relationship between brown dwarf mass, eccentricity, and period for 39 transiting brown dwarf companions including TOI-1994b. The brown dwarfs with orbital periods shorter than 10 days are mostly circularized as expected, with TOI-1994b as an exception.

Ma & Ge (2014) suggests that brown dwarfs can be split into two different populations at  $42.5 M_J$  based on their eccentricity distribution. They found that brown dwarfs with lower masses match the eccentricity distribution for planets, and the higher mass match the eccentricity distribution for stars. The smaller sample of brown dwarfs with masses below  $42.5 M_J$  used in Ma & Ge (2014) followed the trend that the more massive a brown dwarf is, the lower eccentricity it tends to have. The lower-mass brown dwarf eccentricity distribution is also similar to giant planet eccentricity distributions in more recent papers, such as in Rodriguez et al. (2023). Above  $42.5 M_J$ , the eccentricities of brown dwarf companions are more widely distributed. Grieves et al. (2017), Kiefer et al. (2021), and Grieves et al. (2021) conducted a similar analysis using more brown dwarfs and supported the results of Ma & Ge (2014). This split in population may arise from different formation mechanisms, with lower-mass brown dwarfs forming like planets, and higher-mass brown dwarfs forming like stars. Figure 8 displays the relationship between brown dwarf mass, eccentricity, and period for the brown dwarf population, and places a line at  $42.5 M_J$  to show the split in population proposed by Ma & Ge (2014). We note an outlier in the lower-mass brown dwarfs at a mass of around  $36 M_J$  and eccentricity of 0.19. This transiting brown dwarf, EPIC 219388192b, resides in a triple system, which may explain the higher eccentricity (Nowak et al. 2017). The split in population can be clearly seen in Figure 8, with higher-mass brown dwarfs being more distributed in the parameter space.

TOI-1994b has a mass lower than  $42.5 M_J$  and therefore should follow the eccentricity distribution for planets, but it is more eccentric than expected. With the addition of TOI-1994b, it is clear that more transiting brown dwarfs with precise masses are required to verify or refute the population split at  $42.5 M_J$  determined from eccentricity distributions.

The higher eccentricity of TOI-1994b could be potentially explained by gravitational interactions with a stellar companion. We searched for signs of a third object in the speckle imaging for TOI-1994, and found no stellar companions within  $3''$ . We also checked for a slope in the RV data over time, and found that the fit is consistent with a slope of zero over the year of data presented here. Further analysis on a longer time baseline would be necessary to detect the presence of any widely separated stellar companion. Additionally, the Gaia DR3 Renormalized Unit Weight Error (RUWE) indicates whether a single-star model is a good fit for astrometric observations (Belokurov et al. 2020; Lindegren et al. 2021). A RUWE value of  $\sim 1.0$  indicates a good fit, while a value significantly higher than 1.0 could indicate a non-single star. We find that the RUWE value for TOI-1994 is 1.059, suggesting that the single-star model fits the TOI-1994 astrometric observations.

Figure 9 shows the effective temperature and surface gravity of the 39 host stars colored by the mass of their transiting brown dwarf companions. A horizontal line is placed at  $\log(g) = 4.1$  to indicate the transition between main sequence

and evolved hosts as defined by Stassun et al. (2018). There are only six host stars in this set with  $\log(g) < 4.1$  including TOI-1994.

Grunblatt et al. (2018) suggests that close-in giant planets orbiting evolved stars have more eccentric orbits because of tidal interactions with the evolved host. The hot-giant planets may go through an eccentric phase when their orbits shrink faster than they circularize. If this is extended to include low-mass brown dwarfs orbiting evolved stars, it would mean that close-in brown dwarfs orbiting evolved stars also have higher eccentricity. There are currently only six evolved hosts for brown dwarfs. Two of these brown dwarfs, including TOI-1994b, have moderately eccentric orbits that support this hypothesis. Figure 9 shows the host surface gravity versus host effective temperature, with colors representing the mass of the brown dwarf companion. TOI-1994b has the lowest mass of the brown dwarfs transiting evolved stars. It is clear that more brown dwarfs orbiting evolved stars need to be discovered before any real conclusions can be made about how the host evolution effects the brown dwarf in the systems.

### Acknowledgments

This work was funded by NASA XRP grant 80NSSC18K0544 and NSF grant AST2006285. Funding for the TESS mission is provided by NASA's Science Mission Directorate. We acknowledge the use of public TESS data from pipelines at the TESS Science Office and at the TESS Science Processing Operations Center. Resources supporting this work were provided by the NASA High-End Computing (HEC) Program through the NASA Advanced Supercomputing (NAS) Division at Ames Research Center for the production of the SPOC data products. This paper includes data collected by the TESS mission that are publicly available from the Mikulski Archive for Space Telescopes (MAST).

This research has made use of the SIMBAD database, operated at CDS, Strasbourg, France. This research has made use of NASA's Astrophysics Data System Bibliographic Services. This research has made use of the NASA Exoplanet Archive, which is operated by the California Institute of Technology, under contract with the National Aeronautics and Space Administration under the Exoplanet Exploration Program. This research has made use of the Exoplanet Follow-up Observation Program website, which is operated by the California Institute of Technology, under contract with the National Aeronautics and Space Administration under the Exoplanet Exploration Program.

MINERVA-Australis is supported by Australian Research Council LIEF Grant LE160100001, Discovery Grants DP180100972 and DP220100365, Mount Cuba Astronomical Foundation, and institutional partners University of Southern Queensland, UNSW Sydney, MIT, Nanjing University, George Mason University, University of Louisville, University of California Riverside, University of Florida, and The University of Texas at Austin.


We respectfully acknowledge the traditional custodians of all lands throughout Australia, and recognize their continued cultural and spiritual connection to the land, waterways, cosmos, and community. We pay our deepest respects to all Elders, ancestors and descendants of the Giabal, Jarowair, and Kambuwal nations, upon whose lands the Minerva-Australis facility at Mt Kent is situated. G.Z. is supported by Australian

Research Council Discovery Early Career Researcher Award DE210101893.

*Facilities:* TESS, MINERVA-Australis, CTIO:1.5m, SOAR, Exoplanet Archive.

*Software:* Astropy (Astropy Collaboration et al. 2013, 2018, 2022), Lightkurve (Lightkurve Collaboration et al. 2018), EXOFASTv2 (Eastman et al. 2013; Eastman 2017; Eastman et al. 2019), Keplerspline (Vanderburg et al. 2016), Tapir (Jensen 2013).

## ORCID iDs

Emma Page  <https://orcid.org/0000-0002-3221-3874>  
 Joshua Pepper  <https://orcid.org/0000-0002-3827-8417>  
 Duncan Wright  <https://orcid.org/0000-0001-7294-5386>  
 Joseph E. Rodriguez  <https://orcid.org/0000-0001-8812-0565>  
 Robert A. Wittenmyer  <https://orcid.org/0000-0001-9957-9304>  
 Stephen R. Kane  <https://orcid.org/0000-0002-7084-0529>  
 Brett Addison  <https://orcid.org/0000-0003-3216-0626>  
 Timothy Bedding  <https://orcid.org/0000-0001-5222-4661>  
 Brendan P. Bowler  <https://orcid.org/0000-0003-2649-2288>  
 Thomas Barclay  <https://orcid.org/0000-0001-7139-2724>  
 Karen A. Collins  <https://orcid.org/0000-0001-6588-9574>  
 Phil Evans  <https://orcid.org/0000-0002-5674-2404>  
 Jonathan Horner  <https://orcid.org/0000-0002-1160-7970>  
 Eric L. N. Jensen  <https://orcid.org/0000-0002-4625-7333>  
 Marshall C. Johnson  <https://orcid.org/0000-0002-5099-8185>  
 John Kielkopf  <https://orcid.org/0000-0003-0497-2651>  
 Ismael Mireles  <https://orcid.org/0000-0002-4510-2268>  
 PETER PLAVCHAN  <https://orcid.org/0000-0002-8864-1667>  
 Samuel N. Quinn  <https://orcid.org/0000-0002-8964-8377>  
 S. Seager  <https://orcid.org/0000-0002-6892-6948>  
 Avi Shporer  <https://orcid.org/0000-0002-1836-3120>  
 Keivan G. Stassun  <https://orcid.org/0000-0002-3481-9052>  
 Stephanie Striegel  <https://orcid.org/0009-0008-5145-0446>  
 Joshua N. Winn  <https://orcid.org/0000-0002-4265-047X>  
 George Zhou  <https://orcid.org/0000-0002-4891-3517>  
 Carl Ziegler  <https://orcid.org/0000-0002-0619-7639>

## References

- Adams, F. C., & Laughlin, G. 2006, *ApJ*, 649, 1004  
 Addison, B., Wright, D. J., Wittenmyer, R. A., et al. 2019, *PASP*, 131, 115003  
 Astropy Collaboration, Price-Whelan, A. M., Lim, P. L., et al. 2022, *ApJ*, 935, 167  
 Astropy Collaboration, Price-Whelan, A. M., Sipőcz, B. M., et al. 2018, *AJ*, 156, 123  
 Astropy Collaboration, Robitaille, T. P., Tollerud, E. J., et al. 2013, *A&A*, 558, A33  
 Baraffe, I., Chabrier, G., Barman, T. S., Allard, F., & Hauschildt, P. H. 2003, *A&A*, 402, 701  
 Beatty, T. G., Morley, C. V., Curtis, J. L., et al. 2018, *AJ*, 156, 168  
 Belokurov, V., Penoyre, Z., Oh, S., et al. 2020, *MNRAS*, 496, 1922  
 Bodenheimer, P., Lin, D. N. C., & Mardling, R. A. 2001, *ApJ*, 548, 466  
 Boss, A. P., Butler, P. R., & Hubbard, W. B. 2007, *IAUTA*, 26, 183  
 Bowman, D. M., & Kurtz, D. W. 2018, *MNRAS*, 476, 3169  
 Brown, T. M., Baliber, N., Bianco, F. B., et al. 2013, *PASP*, 125, 1031  
 Burrows, A., Hubbard, W. B., Lunine, J. I., & Liebert, J. 2001, *RvMP*, 73, 719  
 Cañas, C. I., Mahadevan, S., Bender, C. F., et al. 2022, *AJ*, 163, 89  
 Carmichael, T. W. 2023, *MNRAS*, 519, 5177  
 Carmichael, T. W., Irwin, J. M., Murgas, F., et al. 2022, *MNRAS*, 514, 4944  
 Carmichael, T. W., Quinn, S. N., Zhou, G., et al. 2021, *AJ*, 161, 97  
 Choi, J., Dotter, A., Conroy, C., et al. 2016, *ApJ*, 823, 102  
 Ciardi, D. R., Beichman, C. A., Horch, E. P., & Howell, S. B. 2015, *ApJ*, 805, 16  
 Collins, K., Quinn, S. N., Latham, D. W., et al. 2018, AAS Meeting Abstracts, 231, 439.08  
 Collins, K. A., Kielkopf, J. F., Stassun, K. G., & Hessman, F. V. 2017, *AJ*, 153, 77  
 Cutri, R. M., Skrutskie, M. F., van Dyk, S., et al. 2003, *yCat*, II/246  
 Cutri, R. M., Wright, E. L., Conrow, T., et al. 2012, *yCat*, II/311  
 Donati, J.-F., Semel, M., Carter, B. D., Rees, D. E., & Collier Cameron, A. 1997, *MNRAS*, 291, 658  
 Dotter, A. 2016, *ApJS*, 222, 8  
 Dupret, M. A., Grigahcène, A., Garrido, R., Gabriel, M., & Scuflaire, R. 2005, *A&A*, 435, 927  
 Eastman, J. 2017, EXOFASTv2: Generalized publication-quality exoplanet modeling code, Astrophysics Source Code Library, ascl:1710.003  
 Eastman, J., Gaudi, B. S., & Agol, E. 2013, *PASP*, 125, 83  
 Eastman, J. D., Rodriguez, J. E., Agol, E., et al. 2019, arXiv:1907.09480  
 Gaia Collaboration, Vallenari, A., Brown, A. G. A., et al. 2023, *A&A*, 674, A1  
 Goldreich, P., & Soter, S. 1966, *Icar*, 5, 375  
 Grether, D., & Lineweaver, C. H. 2006, *ApJ*, 640, 1051  
 Grieves, N., Bouchy, F., Lendl, M., et al. 2021, *A&A*, 652, A127  
 Grieves, N., Ge, J., Thomas, N., et al. 2017, *MNRAS*, 467, 4264  
 Grunblatt, S. K., Huber, D., Gaidos, E., et al. 2018, *ApJL*, 861, L5  
 Guerrero, N. M., Seager, S., Huang, C. X., et al. 2021, *ApJS*, 254, 39  
 Halbwachs, J. L., Mayor, M., Udry, S., & Arenou, F. 2003, *A&A*, 397, 159  
 Huang, C. X., Vanderburg, A., Pál, A., et al. 2020a, *RNAAS*, 4, 206  
 Huang, C. X., Vanderburg, A., Pál, A., et al. 2020b, *RNAAS*, 4, 204  
 Hut, P. 1981, *A&A*, 99, 126  
 Irwin, J., Buchhave, L., Berta, Z. K., et al. 2010, *ApJ*, 718, 1353  
 Irwin, J. M., Charbonneau, D., Esquerdo, G. A., et al. 2018, *AJ*, 156, 140  
 Jackman, J. A. G., Wheatley, P. J., Bayliss, D., et al. 2019, *MNRAS*, 489, 5146  
 Jenkins, J. M. 2002, *ApJ*, 575, 493  
 Jenkins, J. M., Caldwell, D. A., Chandrasekaran, H., et al. 2010, *ApJL*, 713, L87  
 Jenkins, J. M., Tenenbaum, P., Seader, S., et al. 2020, Transiting Planet Search KSCI-19081-003, NASA Ames Research Center  
 Jenkins, J. M., Twicken, J. D., McCauliff, S., et al. 2016, *Proc. SPIE*, 9913, 99133E  
 Jensen, E. 2013, Tapir: A web interface for transit/eclipse observability, Astrophysics Source Code Library, ascl:1306.007  
 Johnson, J. A., Apps, K., Gazak, J. Z., et al. 2011, *ApJ*, 730, 79  
 Kane, S. R., Bean, J. L., Campante, T. L., et al. 2021, *PASP*, 133, 014402  
 Kiefer, F., Hébrard, G., Lecavelier des Etangs, A., et al. 2021, *A&A*, 645, A7  
 Li, J., Tenenbaum, P., Twicken, J. D., et al. 2019, *PASP*, 131, 024506  
 Lightkurve Collaboration, Cardoso, J. V. D. M., Hedges, C., et al. 2018, Lightkurve: Kepler and TESS time series analysis in Python, Astrophysics Source Code Library, ascl:1812.013  
 Lin, Z., Gan, T., Wang, S. X., et al. 2023, *MNRAS*, 523, 6162  
 Lindgren, L., Klioner, S. A., Hernández, J., et al. 2021, *A&A*, 649, A2  
 Lopez, E. D., & Fortney, J. J. 2016, *ApJ*, 818, 4  
 Ma, B., & Ge, J. 2014, *MNRAS*, 439, 2781  
 McCully, C., Volgenau, N. H., Harbeck, D.-R., et al. 2018, *Proc. SPIE*, 10707, 107070K  
 Murphy, S. J., Hey, D., Van Reeth, T., & Bedding, T. R. 2019, *MNRAS*, 485, 2380  
 Nowak, G., Palle, E., Gandolfi, D., et al. 2017, *AJ*, 153, 131  
 Paredes, L. A., Henry, T. J., Quinn, S. N., et al. 2021, *AJ*, 162, 176  
 Phillips, M. W., Tremblin, P., Baraffe, I., et al. 2020, *A&A*, 637, A38  
 Psaridi, A., Bouchy, F., Lendl, M., et al. 2022, *A&A*, 664, A94  
 Ricker, G. R., Winn, J. N., Vanderspek, R., et al. 2015, *JATIS*, 1, 014003  
 Rodriguez, J. E., Quinn, S. N., Vanderburg, A., et al. 2023, *MNRAS*, 521, 2765  
 Sahlmann, J., Ségransan, D., Queloz, D., et al. 2011, *A&A*, 525, A95  
 Schlafly, E. F., & Finkbeiner, D. P. 2011, *ApJ*, 737, 103  
 Schlaufman, K. C. 2018, *ApJ*, 853, 37  
 Schlegel, D. J., Finkbeiner, D. P., & Davis, M. 1998, *ApJ*, 500, 525  
 Sebastian, D., Guenther, E. W., Deleuil, M., et al. 2022, *MNRAS*, 516, 636  
 Smith, J. C., Stumpe, M. C., Van Cleve, J. E., et al. 2012, *PASP*, 124, 1000  
 Spiegel, D. S., Burrows, A., & Milsom, J. A. 2011, *ApJ*, 727, 9  
 Stassun, K. G., Oelkers, R. J., Paegert, M., et al. 2019, *AJ*, 158, 138  
 Stassun, K. G., Oelkers, R. J., Pepper, J., et al. 2018, *AJ*, 156, 102

- Stumpe, M. C., Smith, J. C., Catanzarite, J. H., et al. 2014, [PASP](#), **126**, 100
- Stumpe, M. C., Smith, J. C., Van Cleve, J. E., et al. 2012, [PASP](#), **124**, 985
- Thorngren, D. P., & Fortney, J. J. 2018, [AJ](#), **155**, 214
- Thorngren, D. P., Fortney, J. J., Lopez, E. D., Berger, T. A., & Huber, D. 2021, [ApJL](#), **909**, L16
- Tokovinin, A. 2018, [PASP](#), **130**, 035002
- Tokovinin, A., Fischer, D. A., Bonati, M., et al. 2013, [PASP](#), **125**, 1336
- Twicken, J. D., Catanzarite, J. H., Clarke, B. D., et al. 2018, [PASP](#), **130**, 064502
- Vanderburg, A., Becker, J. C., Kristiansen, M. H., et al. 2016, [ApJL](#), **827**, L10
- Vowell, Noah, Rodriguez, Joseph E., Quinn, Samuel N., et al. 2023, [AJ](#), **165**, 268
- Zhou, G., Winn, J. N., Newton, E. R., et al. 2020, [ApJL](#), **892**, L21
- Ziegler, C., Tokovinin, A., Latiolais, M., et al. 2021, [AJ](#), **162**, 192